An Elastic Deformation Model of High-speed Spindle Units

Igor Aexeevich Zverev[1], In-Ung Eun[2], Young-Kug Hwang[3], Won Jee Chung[4] and Choon Man Lee[4,#]

1 Department of Machine Tools, Moscow State University of Technology (STANKIN), Moscow, Russia
2 Department of Die and Mold Design, Kyonggi Institute of Technology, Siheung, South Korea
3 Graduate School of Mechanical Design and Manufacturing, Changwon National University, Changwon, South Korea
4 Department of Mechanical Design and Manufacturing, Changwon National University, Changwon, South Korea
Corresponding Author / E-mail: cmlee@sarim.changwon.ac.kr, TEL: +82-55-279-7572, FAX: +82-55-267-5142

KEYWORDS : High-speed spindle, Ball bearing, Elastic deformation model

This paper presents an elastic deformation model of a spindle unit (S/U), which takes into account the non-linear properties of high-speed ball bearings (particularly the effect of high rotational speed). For this, a software for the estimation of the S/U elastic deformation properties was developed and intended for use by S/U designers. A computer aided analysis of the model using the developed software was carried out and experiments showed the significant effect of rotational speed, cutting load and bearing axial preload, and showed some new phenomena, from which the criteria for the choice of bearing axial preload is given.

Manuscript received: December 28, 2004 / Accepted: December 28, 2005

NOMENCLATURE

C = Dynamic load-carrying capacity of bearing race way
D_b = Diameter of ball
E = Elastic modulus
F_i = Friction force at inner races
F_o = Friction force at outer races
J = Moment of inertia
K = Stiffness matrix
L = Length of beam
L_f = Nominal fatigue life of a bearing race way
M_g = Gyroscopic moment
P = Vector of the external load
P = Dimensionless parameter ($= \frac{\mathcal{P}_\omega}{\mathcal{P}_\circ}$)
P_o = Assembly preload
P_a = Axial force
P_c = Centrifugal force
P_r = Axial preload
P_ω = Preload at speed ω
Q_i = Contact load at inner races
Q_o = Contact load at outer races
R(Δ) = Reaction vector
S = Cross sectional area
S/U = Spindle Unit
U(Δ) = Potential energy of deformation
Z = Number of balls in the bearing
Δ = Vector of nodal displacement
μ = Frictional coefficient

1. Introduction

One of the most important features of a spindle unit (S/U) is its accuracy. Generally speaking, we can define the S/U accuracy as the stability of the axis of rotation under external and internal disturbances, and measure the accuracy by the S/U resistance to external disturbances and the low level of internal disturbances. There are several sources of S/U disturbances, but one of the principle ones are the cutting forces applied to the spindle while machining. Since a S/U has a limited stiffness, these forces cause spindle axis displacement. Among S/U disturbances we should consider the principal one, i.e., external dynamic forces and internal friction forces. Vibration of a S/U can be represented by the spindle axis vibration spectrum (spectrum of vibrodisplacements) and measured by averaged vibrodisplacement or run-out. It depends on three factors: disturbances (i.e., dynamic forces produced by imperfect bearings and other elements while operation), stiffness of dynamic system, and damping. Another type of phenomena which we can not ignore is heating of the S/U elements in operation because of friction. Heating causes the expansion of S/U parts which varies the spindle position with time, i.e., it causes a loss of S/U accuracy. Heat generation depends on friction in bearings and other elements and thus it is also related with lifetime. We study precision S/Us and our main purpose is to increase S/U accuracy, but here, we do not consider the problem of S/U accuracy directly. We develop a S/U elastic deformation model, which, besides its own importance, forms a principle part of the complex model of S/Us as presented in Fig. 1.

In this paper, we combine the elastic deformation model of a S/U with the model of vibrodisturbances produced by running imperfect bearings and the model of heat generation and transfer and deformations to develop the complex model of a S/U.

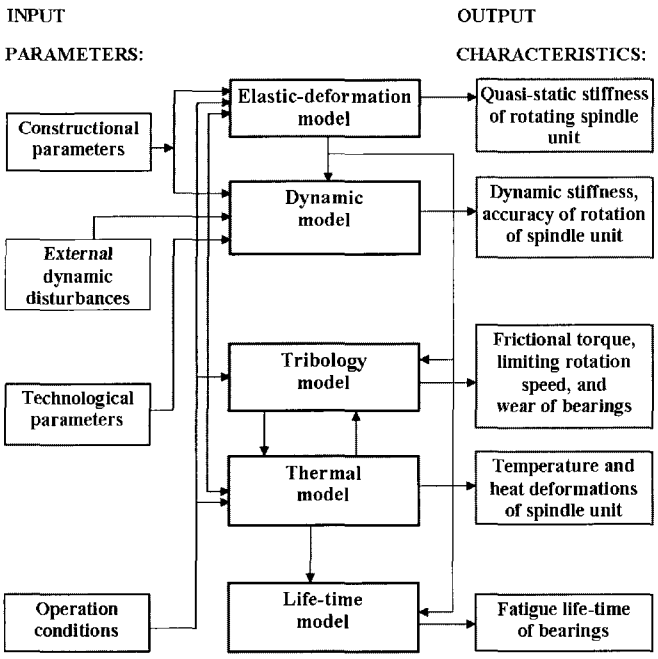

Fig. 1 Diagram of the complex mathematical model of spindle units

2. Theoretical Background of Elastic Deformation Model

When making the analysis, we define stiffness as a measure of spindle rigidity and assume the S/U to be an elastic system. Sometimes, we also use the term 'compliance', which is the inverse of stiffness. The S/U stiffness is a combination of the stiffness of its elements, most of which (spindle, housing, flanges, bushes, rings, etc.) are linear elastic elements, but some are nonlinear. The non-linear elements are ball bearings, whose deformations are mainly produced by the deformation on the contacts between the balls and the races, and these, according to the Hertz theory,[1] depend non-linearly on the contact loads. The picture becomes more complicated, when we make a more detailed analysis of the ball bearing structure, particularly, it turns out that the displacement of the rings under load are related not only to contact deformation, but also to variation of the bearing structure, since a bearing consists of several balls, some part of which can be loaded and some part unloaded. Besides, the equations of bearing equilibrium are the algebraic nonlinear (transcendental) ones because of the trigonometric functions including in unknown decision variables. Thus, bearing elastic deformation properties become non-linear.[2,3] When analyzing high-speed S/Us some new phenomena in bearings appear. These are not only the non-linearity of the elastic properties related to contact deformation in "balls-races", but also the influence of high rotational speed, lubrication, and imperfections of the bearing elements on the bearing properties are also relevant. It is well known that at high rotational speed the centrifugal forces and gyroscopic moments act on the balls and change the bearing properties.[4,5] At the same time, a thin lubricant film appears between balls and races that also changes bearing properties.[6,7] The ball bearings become the main source of S/U vibration and run-out. It is known that the bearings' imperfections, particularly imperfections of their geometry[8] and other imperfections are the main sources of S/U disturbance while rotating, and cause vibration of the S/U.

2.1 Analytical Diagrams of Spindle Units

In order to develop a practically useful elastic deformation model of S/U, we applied the well known finite element method (FEM) and used beam-element analytical diagrams to represent the typical S/U structures as shown in Fig. 2.

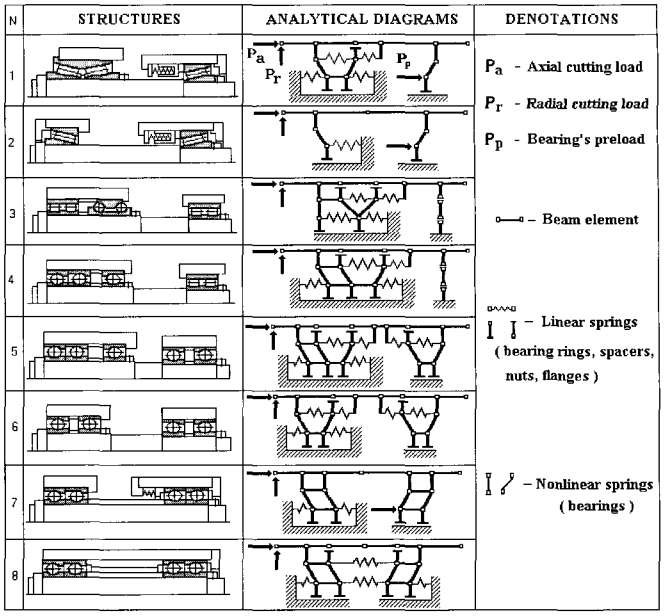

Fig. 2 Typical spindle unit structures and their analytical diagrams

The basic feature and principle advantage of the analytical diagrams shown in Fig. 2 is in their universality: they give us an opportunity to take into account all the principle characteristics of a S/Us structures and the possible conditions of their operation, and solve the problems of statics, dynamics, and heat-transfer.[6] When developing the analytical diagrams for the S/U, we made the following basic assumptions:

1. Spindle unit is a non-linear elastic system of continuous and lumped parameters;
2. Spindle (shaft) is an elastic beam of variable cross section;
3. Ball bearing's stiffness depends non-linearly on load (and preload).

We also introduced the three following types of elastic elements:

1. Beam elements for simulation of the elastic deformation properties of shaft and cylindrical housing;
2. Linear springs for simulation of elastic deformation properties of bearing rings, spacers, lock nuts, and flanges;
3. Nonlinear springs for simulation of nonlinear elastic deformation properties of bearings.

Each node of the elements has three degrees of freedom: radial, axial, and angular.

2.2 Equations of Equilibrium and Method of Solution

The equations of S/U equilibrium, we derive from the general equation of equilibrium of elastic systems:[8]

$$\frac{\partial \mathbf{U}(\Delta)}{\partial \Delta} = \mathbf{P} \tag{1}$$

where $\mathbf{P}$ is the vector of the external loads (3n dimension); $\mathbf{U}(\Delta)$ is the potential energy of S/U deformation; Δ is the vector of nodal displacements (3n dimension), n is the number of nodes in the analytical diagram. The potential energy of each element of the elastic system can be calculated independently. The non-linear equations of S/U equilibrium can be presented in the matrix form after appropriate transformations:

$$\mathbf{K}\cdot\Delta + \mathbf{R}(\Delta) = \mathbf{P} \tag{2}$$

Here, $\mathbf{K} = \sum_{e} \mathbf{K}_e$ is the global stiffness matrix of the linear part of the system (3n×3n dimension); e is the number of beam elements in the analytical diagram; $\mathbf{K}_e$ is the local stiffness matrix of the e-th beam element (6×6 dimension)[9]:

$$\mathbf{K}_e = \begin{bmatrix} \frac{12EJ}{L^3} & \frac{-6EJ}{L^2} & 0 & \frac{-12EJ}{L^3} & \frac{-6EJ}{L^2} & 0 \\ \frac{-6EJ}{L^2} & \frac{4EJ}{L} & 0 & \frac{6EJ}{L^2} & \frac{2EJ}{L} & 0 \\ 0 & 0 & \frac{ES}{L} & 0 & 0 & \frac{-ES}{L} \\ \frac{-12EJ}{L^3} & \frac{6EJ}{L^2} & 0 & \frac{12EJ}{L^3} & \frac{6EJ}{L^2} & 0 \\ \frac{-6EJ}{L^2} & \frac{2EJ}{L} & 0 & \frac{6EJ}{L^2} & \frac{4EJ}{L} & 0 \\ 0 & 0 & \frac{-ES}{L} & 0 & 0 & \frac{ES}{L} \end{bmatrix} \quad (3)$$

E, J, S, L are the elastic modulus, the moment of inertia, the cross-section area, and the length of beam element accordingly; $\mathbf{R}(\Delta) = \mathbf{R}(\Delta, P_c, M_g, Q_i, Q_o, F_i, F_o, \omega)$ is the reactive vector of the non-linear part of the system (3n dimension), where, P_c is the centrifugal force and M_g is the gyroscopic moment acting on the bearing balls; Q_i and Q_o are the contact loads at inner and outer races; F_i and F_o are the friction forces acting on the balls at inner and outer races and preventing gyroscopic sliding of the balls; ω is angular velocity of spindle. The problem of calculation of the bearing reactions $\mathbf{R}(\Delta)$ was considered in detail.[1,4,6,8]

The S/U nodal displacements can be determined from system (2), which can be represented as follows:

$$\mathbf{\Phi}(\Delta) = \mathbf{K}\cdot\Delta + \mathbf{R}(\Delta) - \mathbf{P} = 0 \quad (4)$$

and can be solved using the Newton-Raphson numerical method[11,12]. The general idea of the Newton-Raphson method is to organize the iterative sequence $\Delta_1, \Delta_2, \ldots, \Delta_i$, in such a manner that the (i+1)-th approximation Δ_{i+1} to the exact solution Δ should be determined by the formula $\Delta_{i+1} = \Delta_i - \mathbf{p}_i$, where the correction vector $\mathbf{p}_i$ can be derived from the following system of linear algebraic equations[12]:

$$\frac{\partial \mathbf{\Phi}(\Delta_i)}{\partial \Delta} \cdot \mathbf{p}_i = \mathbf{\Phi}(\Delta_i) \quad (5)$$

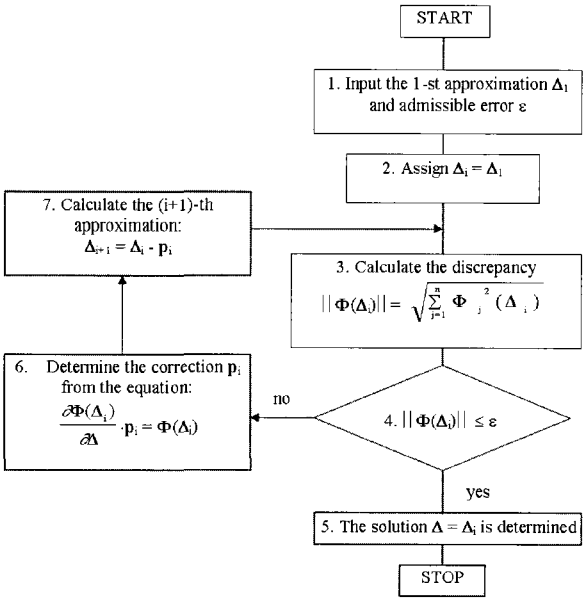

Fig. 3 Algorithm diagram of computation based on the Newton-Raphson method

The algorithm for the solution of system (3) is presented in Fig. 3.

The first approximation Δ_1 and the admissible absolute error ε of the solution, we input into block 1. At the first approximation Δ_1, we assign to the current value Δ_i in block 2 at the beginning of iteration process. The discrepancy $\mathbf{\Phi}(\Delta_i)$, we calculate in block 3 following the formula:

$$||\mathbf{\Phi}(\Delta_i)|| = \sqrt{\sum_{j=1}^{n} \mathbf{\Phi}_j^2(\Delta_i)} \quad (6)$$

where n is the number of equations in the system (3). The decision to terminate the iteration process, we make in block 4 when the condition $||\mathbf{\Phi}(\Delta_i)|| \le \varepsilon$ becomes valid (in block 5, we consider that $\Delta = \Delta_i$), otherwise, (block 6) we determine the correction $\mathbf{p}_i$ by solving system (4). The next (i+1)-th approximation Δ_{i+1}, we calculate in block 7. After that, we repeat all the calculations in blocks 3 and 4. It can happen that no solution will be determined because of computer errors and the discrete character of the iterative process. Therefore, in order to facilitate the choice of the first approximation Δ_1 and the admissible error ε, we recommend following the results of our computer experiment, which showed that we should follow the condition:

$$||\mathbf{\Phi}(\Delta_i)|| \le \varepsilon = 0.01\cdot||\mathbf{P}|| \quad (7)$$

where $||\mathbf{P}||$ is the norm of the vector of external loads. If this recommendation is followed, the process will converge after 7-12 iterations.

2.3 Characteristics of Structures and Operation Conditions of Spindle Units

The elastic deformation properties of S/Us depend on both, the S/U structure and the operation conditions such as external loads, rotational speed, bearing preload, etc.[5,15] When making the analysis, it is necessary to take into account the following characteristics of S/Us:

1. The structure and geometry of the S/U, and the drawing of the bearing mounting;
2. The fit of bearing rings on the shaft and in the housing;
3. The type of bearing preloads (tightly fixed or supported by a spring element).

We consider the S/U structure, geometry of its parts, and diagram of bearing mounting, when developing the S/U analytical diagram (Fig. 2). We consider also the fit of the bearing rings on the shaft and in the housing, when stipulating axial, radial, and angular stiffness of the spring type elements in the diagram. If the bearing ring can freely slide against the surface (Fig. 4 (a)), we consider the axial stiffness of the spring element to be equal to zero. If necessary, we introduce the axial constraint of the ring displacement by means of additional springs 1-3 (Fig. 4 (b)). The fit of the bearing rings in the radial and angular directions, we consider similarly.

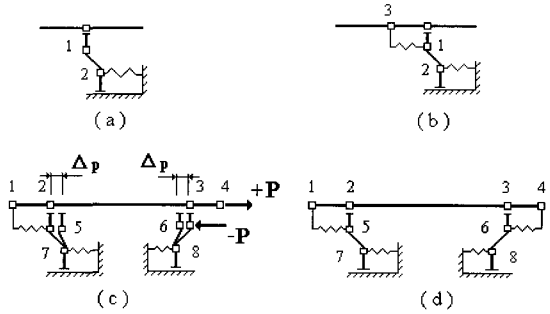

Fig. 4 Fits of bearing rings on the shaft and in the housing (a), (b) and fixed preload (c), (d)

The spring preload (see diagrams 1, 2, and 7 in Fig. 2) provides a constant axial loading of the bearings, and we can take this into account directly when considering the vector of the external loads **P**. The fixed preload provides geometric axial closure of the S/U elements by means of the flanges, lock nuts, and spacers, and we can take this into account in two stages (Fig. 4 (c), (d)). At the first stage, we determine the vector of system deformations Δ_P produced by the external axial loads $+P_4$ and $-P_6$ in the nodes 4 and 6 by solving the system of equations:

$$\mathbf{K}\cdot\Delta_P + \mathbf{R}(\Delta_P) = \mathbf{P}_P \tag{8}$$

where $\mathbf{P}_P$ is the vector of loads when considering the system loaded by the preloads $+P_4$ and $-P_6$ (Fig. 4 (c)). At the second stage, we add the additional constraint 4-6 (the axial spring in Fig. 4 (d)), which simulates a lock nut, and modify the stiffness matrix $\mathbf{K}^*$ as follows:

$$\mathbf{K}^* = \mathbf{K} + \mathbf{K}_{4\text{-}6} \tag{9}$$

where $\mathbf{K}_{4\text{-}6}$ is the extended stiffness matrix of the additional constraint 4-6. The equation of the S/U equilibrium taking into account of the bearing clearance-tightness Δ_P, we present in the form:

$$\mathbf{K}^*\cdot\Delta + \mathbf{R}(\Delta+\Delta_P) = \mathbf{P} \tag{10}$$

where $\mathbf{K}^*$ is the modified stiffness matrix of the linear elastic part of the system in view of the additional constraints; $\mathbf{R}(\Delta+\Delta_P)$ is the vector of the bearing reactions produced by the bearing preloads; $\mathbf{P}$ is the vector of external nodal loads when ignoring the bearing preloads; Δ is the vector of the unknown nodal displacements.

The bearing imperfections produced in manufacturing and assembly, and wear of the bearings cause a relative displacement of the bearing rings Δ_o. In this case, the equation of S/U equilibrium can be represented as follows:

$$\mathbf{K}\cdot\Delta + \mathbf{R}(\Delta+\Delta_P+\Delta_o) = \mathbf{P} \tag{11}$$

where Δ_o is the vector of relative displacements of the bearing rings caused by the bearing imperfections.

3. Elastic Deformation Characteristics of Spindle Units

When studying the S/U properties, we varied rotational speed from 0 up to a value, which corresponds to the speed factor $d\cdot\omega = 1\cdot10^6$ mm·rpm (here d is the average diameter of the front bearing, mm; ω is the maximum rpm); bearing axial preload from light up to heavy value (according to bearing catalogue); and radial load (to simulate cutting force) from 0 up to the double the bearing preload.

3.1 Radial Compliance of Spindle

In the case of fixed and spring type preload, front nose radial displacement with respect to rotational speed and axial preload is presented in Figs. 5 (a) and (b).

The S/U radial compliance decreases from 1.5 to 1.9 times, when the axial preload of the S/U's front bearing increases from super light (100 N) to heavy (900-1100 N) in the case of low rotational speed. It decreases from 1.5 to 2.8 times for the same axial preload variation in the case of high rotational speed (20,000 rpm). When the rotational speed increases from 0 up to 20,000 rpm, the axial compliance increases from 1.5 to 2.3 times at light and super-light preload, and significantly does not vary at heavy preload. The reason for this phenomenon can be explained that the contact force and area in the bearing at heavy preload is greater than that at light preload. This causes a small axial deformation at heavy preload.

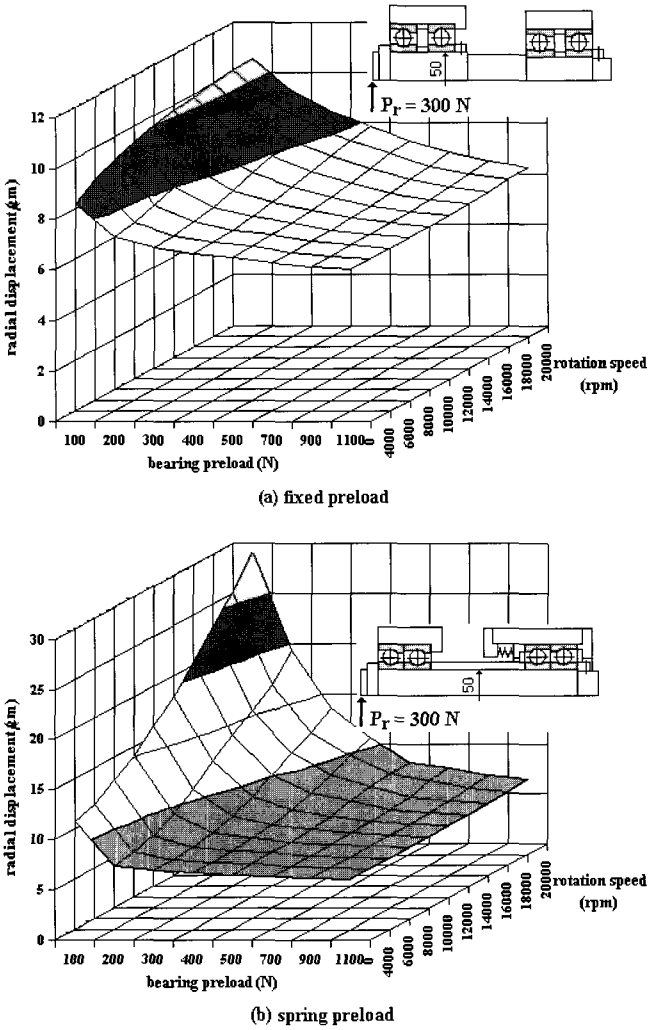

Fig. 5 Radial displacement related to rotational speed and preload

From Fig. 5 it follows that for any rotational speed, we can find a 'critical' value of preload, after which an increase of rotational speed does not cause significant variation of S/U radial stiffness, i.e., there is some kind of radial stiffness 'saturation.' This effect of S/U stiffness saturation, we found in all the S/Us under study. Thus, we can stipulate the following criterion for choosing the S/U bearing preload: the value of preload should not exceed the 'critical' value. Our experiments prove that the 'critical' preload corresponds approximately to the middle value of preload recommended in the ball bearing catalogues or is 10-15 % smaller. In Fig. 5 (a) and (b), we can see that when the speed increases from 0 up to 20,000 rpm, the S/U radial compliance decreases approximately by 2.5 times (in the case of bearing super-light preload of 100 N). The decrease is of 90-100 % in the case of a bearing light preload of 200 N and only by 5 % in the case of bearing heavy preload of 1000-1100 N. The effect of rotational speed on S/U compliance is much greater in the case of spring type preload (when the bearing is preloaded by a relatively soft spring element and one of the bearing rings can slide in the axial direction) than that in the case when all bearing rings are firmly fixed on the shaft and in the housing. We also discovered that though ball bearings have nonlinear elastic deformation properties, S/U radial stiffness turns to be almost constant (does not depend on radial load) which was proved experimentally.[6]

3.2 Axial Preload of Bearings

When S/U rotational speed increases, elastic deformation properties of bearing vary. The dependency of the axial displacement of bearing rings (for the case of spring type preload) and of axial preload, i.e., axial force in the bearing (for the case when the bearing

rings are firmly fixed on the shaft and in the housing) are shown in Fig. 6.

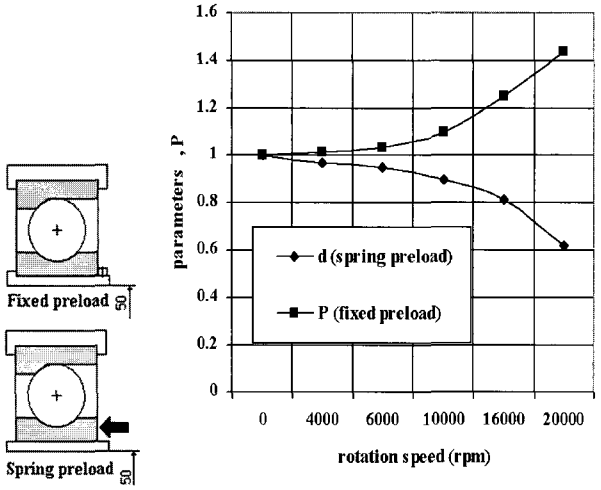

Fig. 6 Dimensionless parameter d and P in dependence on rotational speed

Results are presented for the case when both bearings of S/U were axially preloaded in an assembly by a force of 500 N (that corresponds to the relative axial displacement of bearing rings δ_0 = 16.6 μm). In the case of spring type preload, the additional axial displacement of the rings that appears as the rotational speed increases can be characterize by the dimensionless parameter $\delta = \delta_\omega/\delta_o$, where δ_ω is the relative axial displacement at the speed ω. When ω = 20,000 rotational speed, the bearing rings move apart, and the displacement is equal to 38 % of that provided in the assembly. The real value of preload, in the case when the bearing rings are fixed, we can characterize by the dimensionless parameter $P = P_\omega/P_o$, where P_o is the assembly preload, P_ω is the preload at the speed ω. When the speed increases up to 20,000 rpm, the preload increases by 44 %.

3.3 Axial Displacements of Spindles under High Speed

When analyzing the elastic deformation properties of S/Us using the software developed, we discovered a phenomenon of spindle axial shift with rotational speed. This phenomenon is caused by the centrifugal forces and gyroscopic moments acting on bearing balls and the variation of the bearing elastic deformation properties with rotational speed variation. In the case of a spring type preload of the bearings, an increase of rotational speed causes a displacement of the bearing rings (see i. 3.2) and, thus, an axial displacement of the spindle. In the case when the bearing rings are firmly fixed, centrifugal forces and gyroscopic moments cause the axial preload increase and that also brings to a spindle shift. The results of simulation of the dependence of spindle axial displacement versus rotational speed and preload are presented in Fig. 7. When the spindle does not rotate, the axial force P_a = 200 N (which can be regarded as an axial component of cutting force) causes a spindle displacement in the direction of the applied force. When spindle speeds up to high rotational speed, the centrifugal forces and gyroscopic moments acting on the bearing balls change the elastic deformation properties of the bearings and cause a displacement of the springy supported rings, i.e., it pushes the spindle slightly out of the housing. This effect we term 'negative axial stiffness' of a S/U at high rotational speed.

We performed an experimental study of the effect described using the rig intended for testing of high-speed S/Us (Fig. 8). The S/U housing was mounted in an aerostatic bearing in order to reduce the influence of external disturbances. The spindle was driven by an adjustable motor via a belt transmission. The front bearing was a set of ball bearing having a contact angle of 25°, and the rear bearing was a ball bearing having a contact angle of 15°. The average diameter of bearing is 100 mm. The spindle axial displacements were measured by checking the axial clearance Δ_x between the contactless sensor (mod. TRK/2-5, Hettynger Co.) and the face of measuring mandrel. The sensor signal was input to the amplifier (KWS-73, Hettynger Co.) and then into the spectrum analyzer (mod. 2031, B&K Co.). The sensitivity of the measuring system was 0.1 μm.

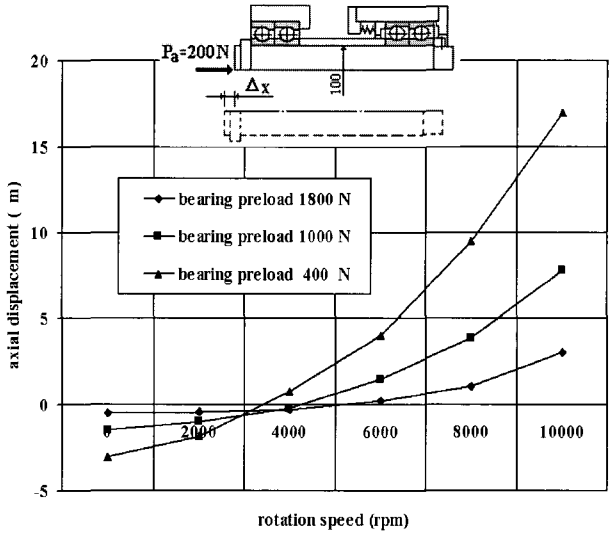

Fig. 7 Axial displacement of the spindle related to rotational speed

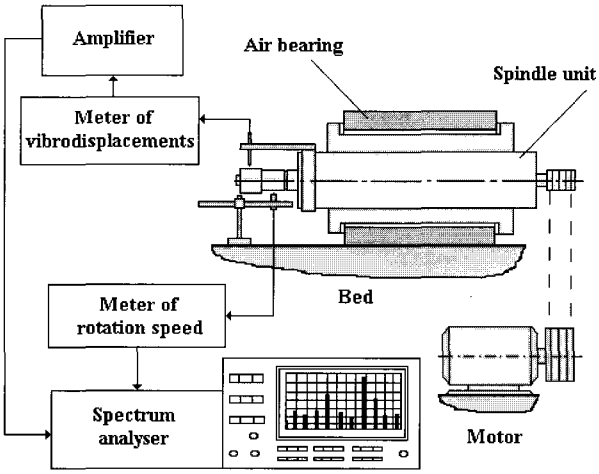

Fig. 8 Layout of the experimental rig

The bearing preload was adjusted by variation of air pressure (see Fig. 9).

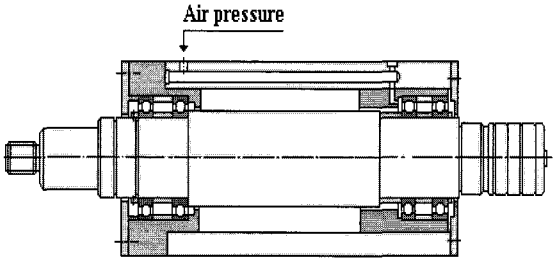

Fig. 9 Experimental spindle unit with variable bearing preload

We made the measurements under three different preloads: 65, 120, and 210 N. After acceleration of the spindle up to 24,000 rpm, we switched off the belt drive and let the spindle rotate freely. The function $\Delta_x=\Delta_x(\omega)$ obtained as a result of these tests is presented in Fig. 10. It shows that the experimental results correspond to the

results of simulation well enough. The maximum discrepancy between the results of simulation and tests does not exceed 17 % at 24,000 rpm, and this discrepancy can be explained by the errors of measurements and imperfections of the model, i.e. the imperfections concerned with approximate mathematical formulation of the kinematical and geometrical bearing characteristics, A. Jones hypothesis of the outer driving-ring[4], ignorable contact deformations in the joints of S/U (the fits of bearing rings on the shaft and in the housing), cross-section distortions of the short-length beams when bending, and others.

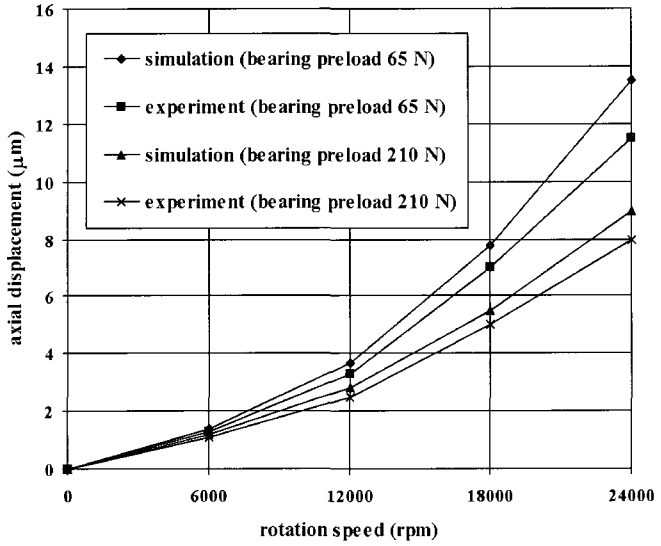

Fig. 10 Axial displacement of the spindle related to rotational speed

3.4 Contact Loads and Fatigue Lifetime of Bearings

The dependence of the maximal contact load (the load on the contacts balls-races) in the S/U front bearing versus rotational speed and preload is presented in Fig. 11. The increase of rotational speed from 0 up to 10,000 rpm and of preload from the super-light value of 0.2 kN up to the heavy value of 1.8 kN, both, result in the increase of maximal contact load.

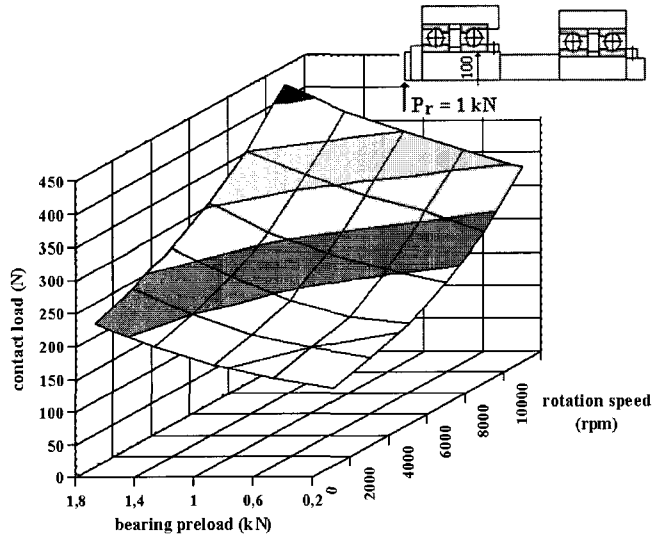

Fig. 11 Maximal contact loads in the front bearing related to preload and rotational speed

An increase of maximal contact load causes a decrease of bearing fatigue life. According to Lundberg–Palmgren' theory[14], a nominal fatigue life of a bearing raceway L_f (probability 90 %) can be estimated by the following formula:

$$L_f = \left(\frac{C}{Q_e}\right)^p \times 10^6 \quad \text{(revolutions)} \tag{12}$$

where C is the dynamic load-carrying capacity of the raceway of bearing, Q_e is the bearing equivalent contact load (p = 3 for ball bearings). In order to estimate the equivalent contact load Q_e using the previously estimated contact loads Q_j, we used the following formula[1]:

$$Q_e = \left[\frac{1}{z}\sum_{j=1}^{z} Q_j^3\right]^{1/3} \tag{13}$$

where z is the number of balls in the bearing. The dependence of fatigue life of an S/U front bearing (spindle diameter 50 mm) on rotational speed and spindle radial load (the bearing preload is accepted to be 500 N) is presented in Fig. 12. The dependence has a nonmonotonic character that can be explained by a nonmonotonic influence of rotational speed and radial loading on the contact loads on the inner raceway of bearing.

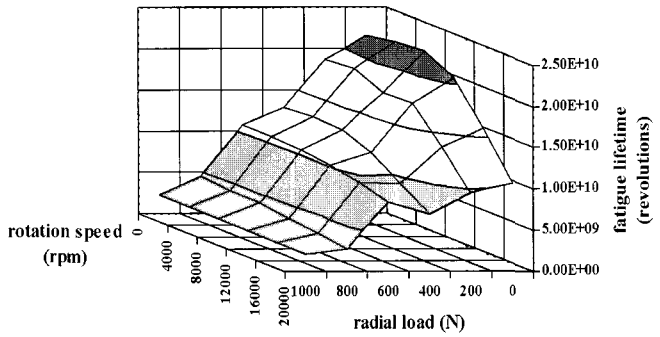

Fig. 12 Fatigue lifetime of the front bearing related to rotational speed and spindle radial load

From Fig. 12 it follows that the effect of radial load on bearing fatigue life is greater than that of rotational speed. The effect of preload and radial load is approximately similar. An increase of speed factor up to $d\cdot\omega = 1.0\cdot10^6$ mm·rpm, in a similar way to an increase of radial load and preload up to the large values results in a decrease of the bearing fatigue life in several orders. Nevertheless, the fatigue life still exceeded 2,000-3,000 hr for all the spindles considered operating under the most severe conditions. Thus, it follows that in high-speed S/Us the bearing fatigue life is not a critical factor.

3.5 Spindle Unit Tolerant Operation Conditions

The recommendations presented in bearing catalogues give the basic criterion for bearing preload and provide a condition of tight contact of balls and races in a bearing loaded by the expected axial and radial loads (including axial preload). However, this condition we find to be insufficient when considering high-speed S/Us. An analysis of the S/U model developed showed us that we should introduce two basic criteria for preload choice. The first one is the traditional one: the bearing balls should be in tight contact with the races under the expected conditions of the S/U operation (i.e., the forces at all of the contacts of balls and races should not be zero). The second one presumes that the bearing balls should not slide against the raceways under the effect of gyroscopic moments acting on the balls at high rotational speed, since sliding can cause ball bearing wear and excessive heating. The sliding can take place in the direction perpendicular to the direction of ball rolling[2,3]. According to this second criterion, the friction torque produced on a bearing raceways

should 'overpower' the gyroscopic moment M_g acting on the balls. That means that the contact forces on the inner ring Q_i and on the outer ring Q_o should satisfy the following condition:

$$\mu \cdot (Q_i + Q_o) \cdot D_b > M_g \quad (14)$$

where μ is the coefficient of sliding friction; D_b is the ball diameter.

The results of the simulation we made for $\mu = 0.06$ are presented in Fig. 13. The figure shows the dependence of minimal preload P_p^{min} required to satisfy both criteria in the S/U front bearing for rotational speed and radial load: $P_p^{min} = P_p^{min}(\omega, P_r)$, where P_p^{min}, ω, P_r are the minimal axial preload, angular velocity of the spindle, and radial load. When the rotational speed is low, the gyroscopic moments are low, and the first criterion works. When the rotational speed is high, the gyroscopic moments acting on bearing balls increase, and the second criterion can start to work. The preload in the S/U bearings should be high enough to eliminate both these phenomena under any of the operation conditions expected.

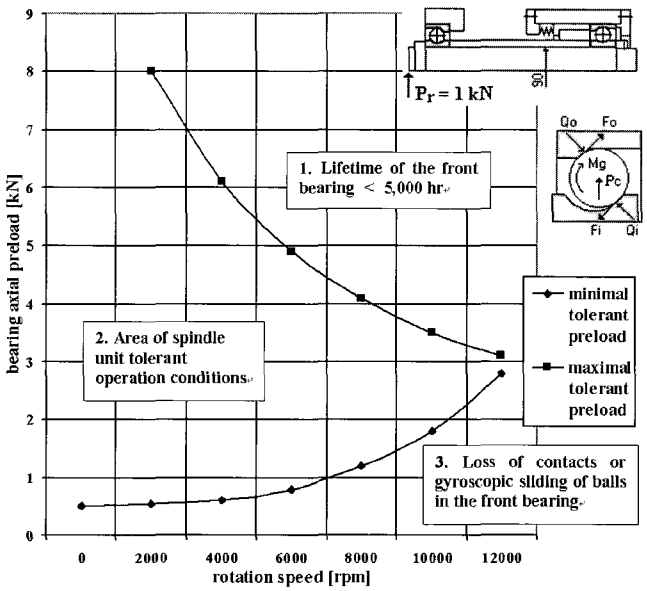

Fig. 13 Minimal and maximal tolerant bearing preloads related to rotational speed

The upper limit of S/U operating conditions, we define by the dependence $P_p^{max} = P_p^{max}(\omega, P_r)$, where P_p^{max}, ω, P_r are the axial preload, angular velocity of the spindle, and radial load under which a required fatigue life of the front bearing will be assured. On the plane "preload – rotational speed" (Fig. 13), we plot three areas (for $P_r = 1$ kN). In the area 1, the lifetime of the front bearing is less than the required value of 5,000 hr. In the area 3, the loss of contact in the front bearing can take place (when $P_r > 1.5 \cdot P_p$) or gyroscopic sliding of the balls can occur. Thus, the areas 1 and 3 are 'forbidden' ones, the acceptable operation conditions are within the area 2.

4. Conclusions

This paper presented an elastic deformation model of S/U running on contact rolling bearings. The model takes into account the different phenomena which change the mechanical properties of the bearings at high rotational speed, and provides analysis of the elastic deformation properties of S/Us. In order to facilitate the analysis, we proposed to use the S/U analytical diagrams and apply FEM and represent the S/Us as a combination of elastic elements of three particular types. As a result of the study, software for computer analysis of the analytical diagrams was developed. The software is intended for use by designers developing high-speed S/Us. We made computer aided studies of precision S/Us, which confirmed the exactness of the model and the software developed. We discovered some unique effects taking place in high-speed S/Us running on ball bearings. These are the following ones:

1. The bearings axial preload and rotational speed can change the stiffness of a S/U significantly. We found out that S/U radial compliance may decrease by 1.5-1.9 times at low rotational speed and by 1.5-2.8 times at high rotational speed ($d \cdot \omega > 1 \cdot 10^6$ mm·rpm), when the bearing axial preload increases from super-light up to heavy. When the rotational speed increases up to $d \cdot \omega = 1 \cdot 10^6$ mm·rpm, the axial compliance increases by 1.5-2.3 times at light and super-light preload, and almost does not vary at heavy preload.
2. The stiffness of S/Us running on ball bearing increases with axial preload of the bearings. However, after exceeding of some 'critical' axial preload, this variation becomes minor even at high rotational speed. We proved that this critical preload corresponds approximately to the middle values of preloads recommended in bearing catalogues or is 10-15% smaller than these.
3. In S/Us having bearings axially preloaded by spring type elements, an increase of rotational speed causes an axial displacement of the spindle relatively the housing, i.e., the spindle shifts in axial direction when the rotational speed changes. In the case of a light preload and a small axial cutting force, the axial displacement can reach 10-15 μm when accelerating from zero to high rotational speed. The effect found was confirmed experimentally.
4. An increase of rotational speed may result in a considerable decrease of bearing fatigue life. However, our estimations proved that the life still exceeds 2,000-3,000 hr for all the spindles considered, i.e., rotational speed does not make strong influence on S/U fatigue life.
5. We estimated the minimal and maximal tolerable axial preloads of S/U ball bearings; for that, we used two criteria: prohibition to lose tight contacts of balls and races, and prohibition of gyroscopic sliding of balls relatively the races.

ACKNOWLEDGEMENT

This work was supported by grant No. RTI04-01-03 from Regional Technology Innovation Program of the Ministry of Commerce, Industry and Energy(MOCIE).

REFERENCES

1. Harris, T. A., "Rolling Bearing Analysis, 3-rd Edition," John Wiley & Sons Inc., 1991.
2. Kingsbury, E., "First order ball-bearing kinematics," Journal of ASME, Vol. 28, No. 2, pp. 22-27, 1985.
3. Hirano, F., "Motion of a ball in angular contact ball bearings," Transactions ASME, Journal of MSE, Vol. 109, No. 8, pp. 425-434, 1965.
4. Jones, A. B., "A General Theory of Elastically Constrained Ball and Radial Roller Bearings under Arbitrary Load and Speed Conditions," Transactions ASME, Journal of MSE, Vol. 82, No. 3, pp. 309-320, 1960.
5. Nakamura, S. and Kakino, Y., "Analysis on preload increment and displacement of a rotating high speed spindle," Journal of the Japan Society of Precision Engineering, Vol. 58, No. 12, pp. 2019-2024, 1992.
6. Zverev, I. A. and Push, A. V., "Spindle Units: Quality and Reliability at Designing (in Russian)," Moscow State Technology Univ. Press, 2000.

7. Lasey, C. L., "High speed bearings for CNC machine tool spindles," Journal of CME, Vol. 4, pp. 51-56, 1983.

8. Juravlev, V. F. and Balmont, V. B., "Mechanics of ball bearings of gyroscopes (in Russian)," Mashinostroenie Edition, Moscow, 1985.

9. Segerlind, L. J., "Applied Finite Element Analysis," John Wiley & Sons Inc., 1996.

10. Sata, T. and Takashima, N., "Dynamic analysis of machine tool structures by the finite element method," Ann. CIRP, Vol. 21, No. 2, pp. 183-191, 1972.

11. Ortega, J. M. and Rheinboldt, W. C., "Iterative Solution of Nonlinear Equations in Several Variables," Academic Press, New-York, 1990.

12. Golub, G. H. and VanLoan, C. F., "Matrix Computations," John Hopkins Univ. Press, Baltimore, 1983.

13. Forsythe, G., Malcolm, M. and Moler, C., "Computer Methods for Mathematical Computations," Prentice-Hall, Englewood Cliffs, New Jersy, 1997.

14. Lundberg, G. and Palmgren, A., "Dynamic Capacity of Rolling Bearings," Acta Politechnica, Mechanical Engineering Series, Vol. 2, No. 4, pp. 50-52, 1952.

15. Chatterjee, S., "Spindle deflection in high-speed machine tools: Modeling and Simulation," International Journal of Advanced Manufacturing Technology, Vol. 11, No. 4, pp. 232-239, 1996.